PCCP

Electronic Supporting Information

Cite this: DOI: 00.0000/xxxxxxxxxx

A chiral metal cluster triggers enantiospecific electron transport.†

Omar Hernández-Montes,[a] Ignacio L. Garzón,[b‡] and J. E. Barrios-Vargas[a]

Contents

S1. Non-Equilibrium Green's Function method 2

S2. Calculations details 3

S3. Relationship between enantiospecific transport and orbital angular momentum 4

S4. Atomic coordinate files 5

List of Figures

S1 Transmission function T(E) for the HB molecule connected to gold electrodes. When T = 0 K, Fermi-Dirac distribution functions $f_{s,d}$ are stair-wise functions (plots colored in blue for f_s and violet for f_d). The net current is proportional to the area under the curve in the interval $\mu_s - \mu_d$; this interval is related to bias potential $\Delta V_{sd} = (\mu_s - \mu_d)/|e|$. 3

S2 Molecular junctions for a) *para*-terphenyl and b) *meta*-terphenyl configurations. c) Transmission function in logarithmic scale for terphenyl in *para* (yellow curve) and *meta* (red curve) configurations. A transmission fall-down around two orders of magnitude is registered for *meta* structure in comparison with *para* case at the Fermi level, indicating the presence of destructive quantum interference for the former and constructive for the last one, respectively. 4

S3 Visualization of chiral-modified molecular junctions for a) achAu$_{34}$-HBR and b) achAu$_{34}$-HBL in the zx-plane, the plots of their difference in PDOS for p-like orbitals, p_x (orange), p_y (blue), p_z(red) for c) carbon atoms and d) sulfur atoms of HB molecule: in these plots no significant difference is observed, so, no change in orbital angular momentum of transmitted electron occurs. 5

S4 Visualization of chiral-modified molecular junctions for a) chAu$_{34}$-HBR and b) chAu$_{34}$-HBL in the zx-plane, the plots of their difference in PDOS for p-like orbitals, p_x (orange), p_y (blue), p_z(red) for c) carbon atoms and d) sulfur atoms of HB molecule: in these plots significant difference is observed for the p_y orbital, so, this indicates a change in y-direction in the path of electron transmission. 5

[a] *Departamento de Física y Química Teórica, Facultad de Química, Universidad Nacional Autónoma de México, Ciudad de México 04510, México, E-mail: omar.hdz.mon@gmail.com, j.e.barrios@gmail.com*

[b] *Instituto de Física, Universidad Nacional Autónoma de México, Apartado Postal 20-364, Ciudad de México 01000, México, E-mail: garzon@fisica.unam.mx*

S1. Non-Equilibrium Green's Function method

We use Non-Equilibrium Green's Function method to characterize electronic transport. This method is based on Green's function that is defined as,[1]

$$[G] = [EI - H_{\mathrm{mol}} - \Sigma_{\mathrm{s}} - \Sigma_{\mathrm{d}}]^{-1}\,, \tag{1}$$

where $\Sigma_{\mathrm{s,d}}$ are the self-energies that describe the coupling of the molecule with source and drain electrodes, respectively. H_{mol} is the molecular Hamiltonian in the gas phase; particularly, we have made use of density functional theory (DFT), so H_{mol} is the Khon-Sham Hamiltonian of our system: $H_{\mathrm{KS}} = p^2/2m + V_{\mathrm{KS}}[n]$ where Kohn-Sham potential V_{KS} is a functional of electron density n:

$$V_{\mathrm{KS}}[n] = V_{\mathrm{ext}}[n] + V_{\mathrm{H}}[n] + V_{\mathrm{xc}}[n]\,. \tag{2}$$

Once we have defined the Hamiltonian and self-energies in our molecular junction, we can determine the transmission function, which is defined in terms of Green's function, G, by[2],

$$\mathrm{T(E)} = \mathrm{Tr}[\Gamma_{\mathrm{s}} G \Gamma_{\mathrm{d}} G^{\dagger}]\,, \tag{3}$$

where $\Gamma_{\mathrm{s,d}}$ are the broadening matrices defined as: $\Gamma_{\mathrm{s,d}} = i[\Sigma_{\mathrm{s,d}} - \Sigma_{\mathrm{s,d}}^{\dagger}]$. We use the Landauer formalism for calculating the current in the molecular junction,

$$I = \frac{2e}{h}\int \mathrm{T(E)}\big[f_{\mathrm{s}}(E-\mu_{\mathrm{s}}) - f_{\mathrm{d}}(E-\mu_{\mathrm{d}})\big]\mathrm{dE}\,, \tag{4}$$

where $f_{\mathrm{s,d}}$ are the Fermi's functions for the source and drain contacts, respectively, and $\mu_{\mathrm{s,d}}$ are its chemical potentials; at $T = 0$ K, these functions are step functions, so the difference among them is,

$$f_{\mathrm{s}}(E) - f_{\mathrm{d}}(E) = \begin{cases} 1, & \text{if} \quad \mu_{\mathrm{s}} > E > \mu_{\mathrm{d}} \\ 0, & \text{otherwise} \end{cases}\,, \tag{5}$$

so the electric current is given by[3],

$$I = \frac{2e}{h}\int_{\mu_{\mathrm{s}}}^{\mu_{\mathrm{d}}} \mathrm{T(E)dE}\,. \tag{6}$$

The electric current at T = 0 K is the area under the curve of the function T(E) in the interval range μ_{s}-μ_{d}; the integral outside that range is zero. The bias voltage is the integration interval given by $\Delta \mathrm{V_{sd}} = (\mu_{\mathrm{s}} - \mu_{\mathrm{d}})/|e|$, this zero bias approximation at low temperatures is depicted in Figure S1. We use TranSIESTA[4] and TBtrans codes to obtain the Green's and transmission functions, respectively.

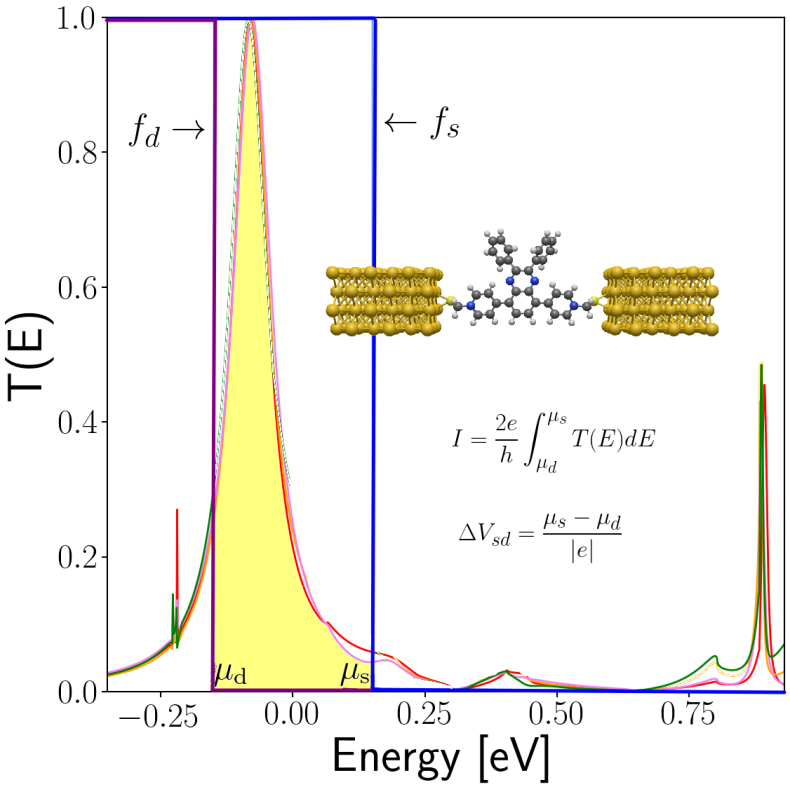

Figure S1 Transmission function T(E) for the HB molecule connected to gold electrodes. When $T = 0$ K, Fermi-Dirac distribution functions $f_{s,d}$ are stair-wise functions (plots colored in blue for f_s and violet for f_d). The net current is proportional to the area under the curve in the interval $\mu_s - \mu_d$; this interval is related to bias potential $\Delta V_{sd} = (\mu_s - \mu_d)/|e|$.

S2. Calculations details

All calculations were carried out using a GGA functional in the PBE approximation: first, before transport calculations, we performed geometric optimization for electrodes, chiral metal cluster Au_{34}, and organic molecules using the DFT-based SIESTA[5,6] code, with a set of DZP basis. Then, to construct molecular junctions, we used the thiol group as the anchoring group, which is known to be effective in binding molecules to Au electrodes; in particular, we bound viologens, placing the sulfur atom in a bridge position with Au FCC electrodes, in the same way as attaching to the Au_{34} cluster case[7]. The equilibrium distance between the Au electrode and the Au_{34} cluster was determined adiabatically. Furthermore, for the equilibrium distance between the chiral cluster Au_{34} and the viologen, we considered a distance Au-S of 2.6 Åpreviously reported[7]. Lastly, for transport calculations in TranSIESTA, we used a mesh cutoff of 340 Ry, also a Monkhorst-Pack grid [100, 1, 1], this means that we employed 100 k-points along the transport direction (along x axis), and for the transverse directions in the transport path (y and z directions) just 1 k-point (this is, just the gamma point).

To test the calculation parameters, we qualitatively reproduce the results reported in Ref. 8. Figure S2 displays the transmission function (in logarithmic scale) for the *para* and *meta* configurations of terphenyl. From it, it is possible to observe that we can reproduce constructive quantum interference for the *para* connection and destructive interference for the *meta* case. Destructive quantum interference is a fall-down in transmission function of several magnitude orders; in this case, there is a difference of more than two orders of magnitude between the minimum of the *para* case and the *meta* case, which is in agreement with the results reported by

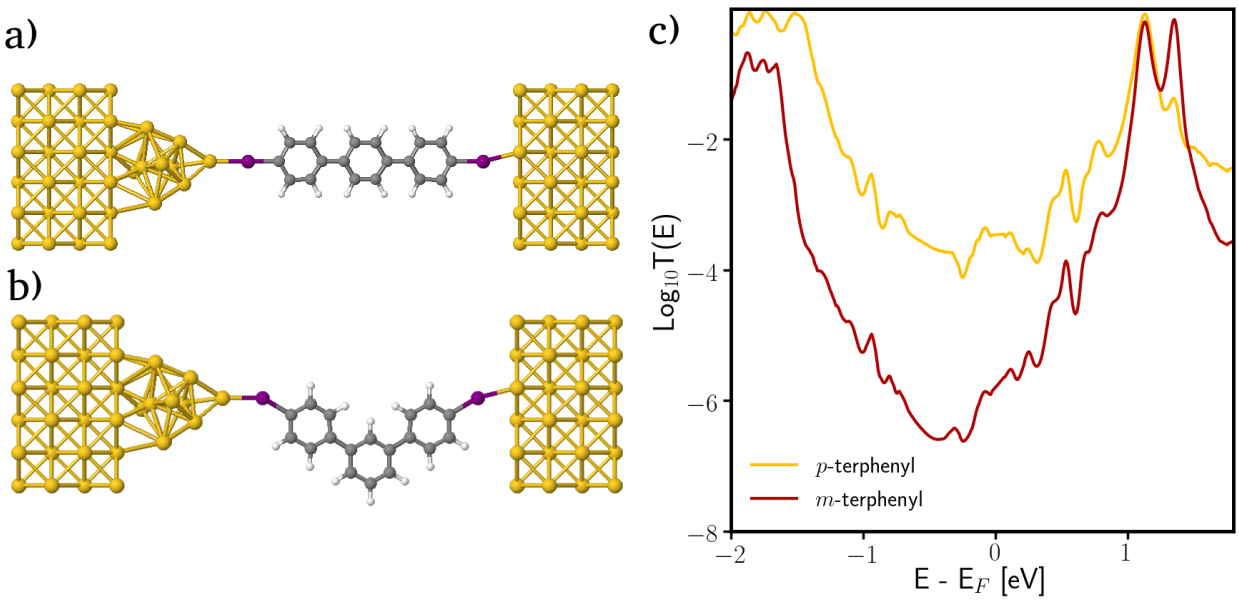

Figure S2 Molecular junctions for a) *para*-terphenyl and b) *meta*-terphenyl configurations. c) Transmission function in logarithmic scale for terphenyl in *para* (yellow curve) and *meta* (red curve) configurations. A transmission fall-down around two orders of magnitude is registered for *meta* structure in comparison with *para* case at the Fermi level, indicating the presence of destructive quantum interference for the former and constructive for the last one, respectively.

Li *et al.* in Ref. 8.

S3. Relationship between enantiospecific transport and orbital angular momentum

To investigate the relationship of orbital angular momentum and the enantiospecific electron transport, further calculations and analysis were performed. In particular, here we calculated the difference in the projected density of states (PDOS) between the R and L-cases as follows:

$$\text{Difference PDOS}(n,l,m_l) = \text{PDOS}(n,l,m_l)_{\text{HBR}} - \text{PDOS}(n,l,m_l)_{\text{HBL}} \tag{7}$$

The difference in PDOS is presented below in both the achiral- and chiral-modified molecular junctions. We show for the achiral case (see Figure S3, below) in the p-like orbitals of carbon and sulfur atoms, a non-significant difference among HBL and HBR cases occurs (see Figure S3-c,d respectively). In contrast, in the case of the chiral-modified molecular junctions, a significant difference in PDOS between the HBR and HBL cases exists, in particular for C $2p_y$ and S $3p_y$ orbitals (see blue curves in Figures S4-c,d respectively). So, these results indicate that the p-like orbitals of the carbon and sulfur atoms are not different when an achiral cluster is present, but the opposite behavior is obtained when a chiral cluster modifies the gold electrode.

Also, we highlight the relevance of the orbital p_y: meanwhile, the difference PDOS for p_x and p_z is tiny, and the main difference occurs in the orbital p_y, indicating that the chiral cluster chAu_{34} deviates the electron transmission path in the y-direction, which is a perpendicular direction to the plane zx, where chirality is present. Lastly, the deviation's degree is upon whether the molecule HB is R- or L-handed. These results provided further insights into the relationship of the enantiospecific electron transport with the filtering of orbital angular momentum.

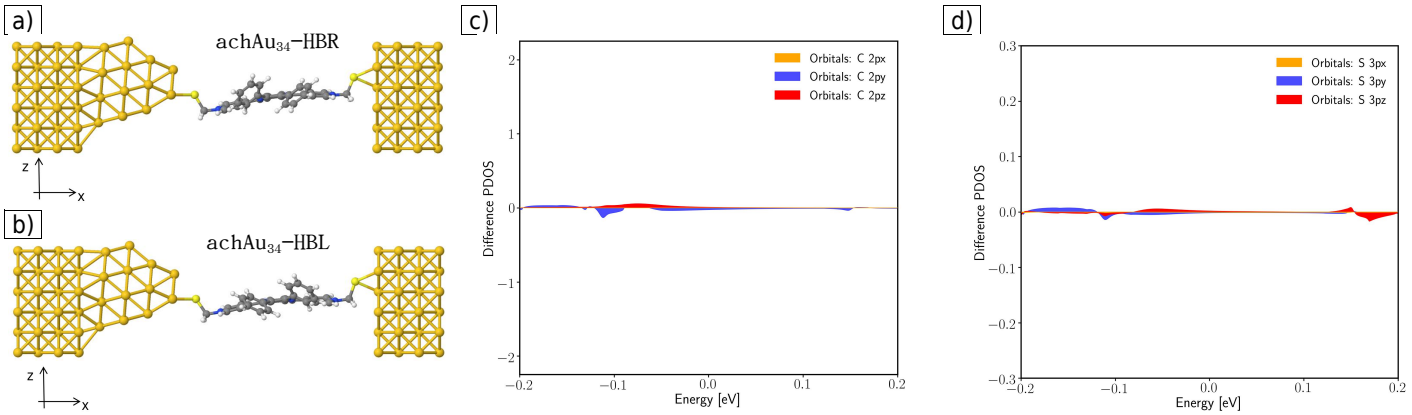

Figure S3 Visualization of chiral-modified molecular junctions for a) achAu$_{34}$-HBR and b) achAu$_{34}$-HBL in the zx-plane, the plots of their difference in PDOS for p-like orbitals, p_x (orange), p_y (blue), p_z(red) for c) carbon atoms and d) sulfur atoms of HB molecule: in these plots no significant difference is observed, so, no change in orbital angular momentum of transmitted electron occurs.

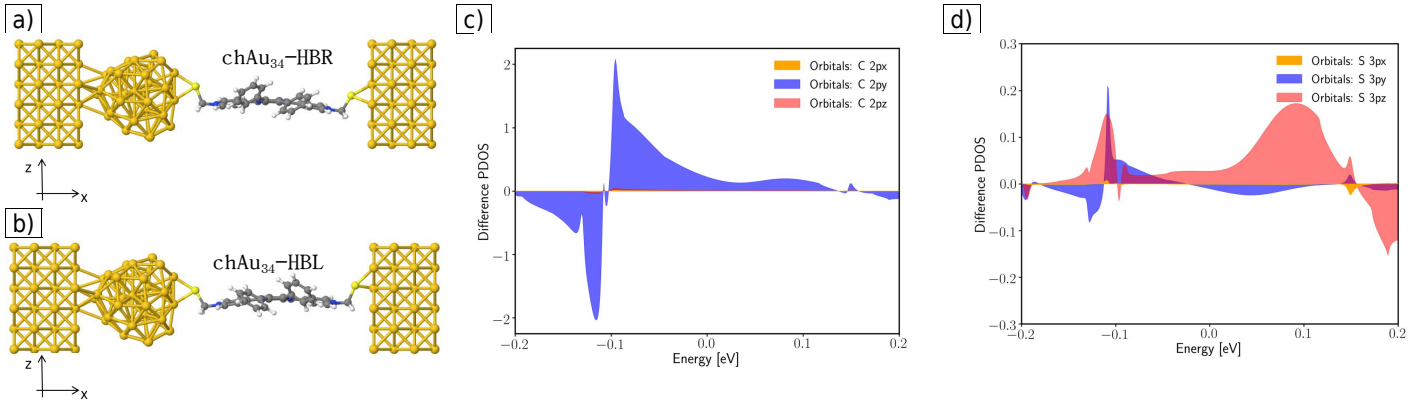

Figure S4 Visualization of chiral-modified molecular junctions for a) chAu$_{34}$-HBR and b) chAu$_{34}$-HBL in the zx-plane, the plots of their difference in PDOS for p-like orbitals, p_x (orange), p_y (blue), p_z(red) for c) carbon atoms and d) sulfur atoms of HB molecule: in these plots significant difference is observed for the p_y orbital, so, this indicates a change in y-direction in the path of electron transmission.

S4. Atomic coordinate files

The atomic coordinates of bonded viologens to chAu$_{34}$ are available in:

- for chAu$_{34}$-HBR:
  https://github.com/jebarriosvargas/PCCP_D3CP04581A/blob/2ac6373d2bffaf2a9e8e92ef24416b3a99a05376/au34_hb3R.pdb
- for chAu$_{34}$-HBL:
  https://github.com/jebarriosvargas/PCCP_D3CP04581A/blob/2ac6373d2bffaf2a9e8e92ef24416b3a99a05376/au34_hb3L.pdb

The aim of supplying this information is:

- To provide a guide where the chirality emerges in viologens + Au$_{34}$ systems.
- To show the bridge-bonded sulfur anchoring group and to prove that the connection is equivalent in both the L- and the R- systems.

Notes and references

1 S. Datta, *Quantum transport: atom to transistor*, Cambridge university press, 2005.

2 S. Datta, *Electronic Transport in Mesoscopic Systems*, Cambridge University Press, 1995.

3 S. Datta, *Nanotechnology*, 2004, **15**, S433.

4 M. Brandbyge, J.-L. Mozos, P. Ordejón, J. Taylor and K. Stokbro, *Phys. Rev. B*, 2002, **65**, 165401.

5 J. M. Soler, E. Artacho, J. D. Gale, A. García, J. Junquera, P. Ordejón and D. Sánchez-Portal, *J. Condens. Matter Phys.*, 2002, **14**, 2745.

6 A. García, N. Papior, A. Akhtar, E. Artacho, V. Blum, E. Bosoni, P. Brandimarte, M. Brandbyge, J. I. Cerdá, F. Corsetti, R. Cuadrado, V. Dikan, J. Ferrer, J. Gale, P. García-Fernández, V. M. García-Suárez, S. García, G. Huhs, S. Illera, R. Korytár, P. Koval, I. Lebedeva, L. Lin, P. López-Tarifa, S. G. Mayo, S. Mohr, P. Ordejón, A. Postnikov, Y. Pouillon, M. Pruneda, R. Robles, D. Sánchez-Portal, J. M. Soler, R. Ullah, V. W.-z. Yu and J. Junquera, *J. Chem. Phys.*, 2020, **152**, 204108.

7 J. J. Pelayo, I. Valencia, G. Díaz, X. Lopez-Lozano and I. L. Garzón, *Eur. Phys. J. D*, 2015, **69**, 1–7.

8 Y. Li, M. Buerkle, G. Li, A. Rostamian, H. Wang, Z. Wang, D. R. Bowler, T. Miyazaki, L. Xiang, Y. Asai, G. Zhou and N. Tao, *Nat. Mater*, 2019, **18**, 357–363.